

HiSST: 4th International Conference on High-Speed Vehicle Science Technology 22 -26 September 2025, Tours, France



New Insights into The Temperature Jump of C/SiC Composites under Extreme Aerothermal Conditions

Yifan Fu¹, Xin Lin², Junjie Pan³ Zezhong Wang⁴ and Xilong Yu⁵

Abstract

Carbon fiber-reinforced silicon carbide (C/SiC) composites are essential for the thermal protection systems of reusable hypersonic vehicles. Their high-temperature performance relies on a protective silica (SiO₂) layer, but this can be compromised by a sudden, hazardous increase in surface temperature, known as "temperature jump". The complex gas-surface interaction mechanisms driving this phenomenon remain inadequately understood. This study presents an experimental investigation of the temperature jump mechanism on a C/SiC composite. Experiments were conducted in a 1.2 MW plasma wind tunnel under high-enthalpy (42.8 MJ/kg) conditions. A designed two-stage thermal loading procedure successfully induced a temperature jump from ~2000 K to ~2400 K.By employing a multidiagnostic approach combining pyrometry, Scanning Electron Microscopy (SEM), Optical Emission Spectroscopy (OES), and quantitative Laser Absorption Spectroscopy (LAS), the gas-surface interactions were probed. The results demonstrate that the temperature jump is associated with a transition from a passive to an active oxidation regime. SEM analysis confirmed the failure of the protective SiO2 layer, exposing the underlying material to aggressive ablation. The time-resolved LAS measurements revealed a synchronous and sharp increase in both the translational temperature and the number densities of near-body O and N atoms. This increase in reactant density is attributed to a reduced net consumption rate during active oxidation. Concurrently, OES registered a surge in emission from reaction products (Si, CN), corroborating the shift to a vigorous ablation mode. By integrating time-resolved, quantitative measurements of reactant densities with spectral monitoring of reaction products and detailed microstructural analysis, this work offers new insights on the temperature jump phenomenon, providing valuable data to advance the understanding and predictive modeling of C/SiC materials in extreme aerothermal environments.

Keywords: C/SiC composite, temperature jump, laser absorption spectroscopy, number density, high-enthalpy

Nomenclature

 ν – frequency

 I_0 – incident laser intensity

I_r – transmitted laser intensity

under Extreme Aerothermal Conditions

 k_{ν} – spectral absorption coefficient

HiSST-2025-#296 New Insights into The Temperature Jump of C/SiC Composites

Page | 1

¹ State Key Laboratory of High Temperature Gas Dynamics, Institute of Mechanics, Chinese Academy of Sciences, 100190 Beijing China; School of Engineering Science, University of Chinese Academy of Sciences, 100049 Beijing China; fuyifan@imech.ac.cn

² State Key Laboratory of High Temperature Gas Dynamics, Institute of Mechanics, Chinese Academy of Sciences, 100190 Beijing China, linxin_bit@imech.ac.cn (Corresponding Author)

³ State Key Laboratory of High Temperature Gas Dynamics, Institute of Mechanics, Chinese Academy of Sciences, 100190 Beijing China, 1239808187@gg.com

⁴ State Key Laboratory of High Temperature Gas Dynamics, Institute of Mechanics, Chinese Academy of Sciences, 100190 Beijing China, wangzezhong@imech.ac.cn

⁵ State Key Laboratory of High Temperature Gas Dynamics, Institute of Mechanics, Chinese Academy of Sciences, 100190 Beijing China; School of Engineering Science, University of Chinese Academy of Sciences, 100049 Beijing China, xlyu@imech.ac.cn

L – absorbing pass length

 S_{μ} – line strength of transition

 n_i – lower state number density

 n_0 – total number density

 ϕ_0 – line-shape function

 λ_0 – central wavelength of transition

A – Einstein coefficient of transition

 q_i – lower state degeneracy

 g_{μ} – upper state degeneracy

h - Planck constant

 $k_{\scriptscriptstyle R}$ – Boltzmann constant

 Δv_{D} – Doppler width

 T_{rr} – translational temperature

 $\nu_{\scriptscriptstyle 0}$ – central wavenumber of transition

 E_{i} – lower state energy

Q(T) – electronic partition function of atoms

1. Introduction

During atmospheric reentry or hypersonic cruise, aircraft experience significant aerodynamic heating due to shock wave compression and viscous friction, leading to the excitation, dissociation, and ionization of atmospheric constituents. In this high-enthalpy environment, thermal protection materials must simultaneously withstand high heat fluxes and erosion from chemically active particles. Their performance directly determines the structural integrity and mission reliability of the aircraft. Carbon fiber-reinforced silicon carbide (C/SiC) composites, valued for their low density, high thermal shock resistance, and superior oxidation resistance, are considered ideal candidates for next-generation thermal protection materials and have been applied in the thermal protection systems of spacecraft such as the IXV and the X-37B [[1-3]]. However, C/SiC materials are susceptible to a phenomenon known as the "temperature jump" in high-enthalpy environments, characterized by a sudden increase of several hundred Kelvin in surface temperature accompanied by severe ablation. This phenomenon, as reported in several studies [4-5], poses significant challenges for thermal protection systems.

The temperature jump phenomenon in C/SiC materials was first discovered in the 1990s through arcjet wind tunnel experiments [6] and has since drawn sustained attention in the field of thermal protection. Researchers have found that material oxidation behavior plays a critical role in the temperature jump [7-9], particularly during the transition from passive to active oxidation. During this transition, the failure of the SiO₂ protective layer leads to the accelerated direct oxidation of SiC. When "passive oxidation" dominates, the dense SiO2 glass layer formed by SiC reacting with oxygen effectively suppresses oxygen diffusion and reduces ablation rates. However, as thermal effects accumulate, the SiO₂ protective layer fails, reaction changes into an "active oxidation" phase dominated by direct SiC oxidation. Nonetheless, experiments in pure oxygen environments indicate that the heat contribution from oxidation alone is insufficient to explain this phenomenon. The exothermic catalytic reaction of SiC with nitrogen atoms, therefore, cannot be overlooked. Additional studies have explored potential causes of the temperature jump from various perspectives, such as reaction enthalpy values, flow field conditions, and changes in material surface properties and recombination [10-11], indicating that the catalytic recombination of gaseous silicon with atomic nitrogen is a key contributing factor to the abrupt temperature change. Although no unified theory has yet emerged, there is a general consensus that this rapid temperature jump exceeds the scope of simple heat conduction. It is fundamentally the result of complex physicochemical processes involving the interaction between highenthalpy flows and the material surface within the boundary layer. Processes such as the formation and degradation of SiO₂ on the material surface, SiC layer ablation, and C fiber exposure are closely associated with the temperature jump [3][5][12-17]. These processes are not only triggered by specific physicochemical reactions but are also significantly influenced by the surface roughness and structural evolution of the material, which in turn affect the chemical reaction processes in the near-body region. The complexity of the temperature jump stems from the coupled chemical reactions within the boundary layer, where catalytic, oxidation, and nitridation reactions involving atomic components interact competitively. However, traditional methods like scanning electron microscopy (SEM) analysis only provide post-mortem microstructural and chemical composition information. Consequently, they cannot capture transient changes in parameters, such as component density, during the reaction, which poses a major challenge for current research. Although some researchers have attempted to interpret the temperature jump from different perspectives by obtaining radiation intensities of Si and CN via optical

emission spectroscopy (OES) [5][7-8], the indirect nature of excited-state measurements limits direct parameter quantification, leaving such studies without effective quantitative characterization methods.

Non-invasive optical spectroscopic diagnostic techniques offer powerful tools for quantitatively analyzing the chemical processes underlying the temperature jump. Among these, laser absorption spectroscopy (LAS) has been successfully applied in high-enthalpy experimental facilities such as ICP wind tunnels, arc-jet wind tunnels, and shock tubes, enabling precise measurements of the number density and translational temperature of key active particles (e.g., O atoms, N atoms) in dissociated gases [18-21]. Admittedly, absorption spectroscopy is a line-of-sight measurement technique, meaning that a single laser beam can hardly provide high-spatial-resolution two-dimensional or three-dimensional distribution information. However, laser absorption spectroscopy is uniquely suited for investigating the gas—surface interactions that drive the temperature jump, which is the central focus of this research. The core reaction zone of the boundary layer is extremely thin and situated immediately adjacent to the material surface. By arranging the absorption spectroscopy optical path parallel and proximate to the material surface, it is possible to accurately capture parameter changes of key components (such as O and N atoms) within this near-body region. This enables the data to be correlated with reaction processes like oxidation and catalysis within the boundary layer, as confirmed in previous studies [22-23].

In this study, atomic laser absorption spectroscopy was employed to analyze the gas composition near the C/SiC material surface, with the aim of achieving quantitative measurements of oxygen and nitrogen atom translational temperature and number density to investigate the temperature jump mechanism. Utilizing a 1.2 MW plasma wind tunnel, a temperature jump scenario for C/SiC materials under highenthalpy conditions was recreated. By simultaneously measuring the absorption spectra of oxygen and nitrogen atoms near the C/SiC surface using coupled lasers, this study quantitatively determined the changes in oxygen and nitrogen atom number densities and non-equilibrium temperatures. These insitu measurements were supplemented by emission spectroscopy to capture radiative signals from the reaction zone. Following the experiments, the samples were subjected to post-test analysis using scanning electron microscopy (SEM) to characterize their resulting microstructures and elemental compositions. This research aims to establish a deeper understanding of the temperature jump phenomenon in Cshiji/SiC materials.

2. Principles of Laser Absorption Spectroscopy

Laser Absorption Spectroscopy (LAS) was employed to perform in-situ measurements of the translational temperature and number density of atomic oxygen and nitrogen in the near-body region. The technique is based on the Beer-Lambert law, which describes the attenuation of monochromatic light as it passes through an absorbing medium. The relationship between the incident intensity $I_0(\nu)$ and the transmitted intensity $I_t(\nu)$ is given by:

$$\frac{I_t(v)}{I_0(v)} = exp(-\alpha_v) = exp(-k_v \cdot L)$$
 (1)

where k_{ν} [cm⁻¹] is the spectral absorption coefficient at frequency, L [cm] is the absorption path length, corresponding to the diameter of the sample's plasma-exposed surface in this work. The absorbance α_{ν} , is determined experimentally. For a uniform medium, the absorption coefficient is a product of the line strength of the transition, the number density of the absorbing species, and a lineshape function:

$$\alpha_{v} = S_{u} n_{l} \phi_{v} L \tag{2}$$

Where, S_{lu} [cm⁻¹/(molecule·cm⁻²)]is the line strength of the transition from a lower energy state I to an upper state u, n_{ll} [cm⁻³]is the number density of atoms in the lower state I, and ϕ_{lu} [cm]is the normalized lineshape function.

The translational temperature is derived from the profile of the absorption lineshape. Under the high-temperature, low-pressure conditions of the plasma wind tunnel, the lineshape is primarily governed by the thermal motion of the atoms, resulting in Doppler broadening [23]. The corresponding lineshape is described by a Gaussian function:

HiSST-2025-#296 Page | 3

$$\phi_D = \frac{2}{\Delta V_D} \sqrt{\frac{\ln 2}{\pi}} \exp\left(-4 \ln 2 \left(\frac{V - V_0}{\Delta V_D}\right)^2\right)$$
 (3)

The full width at half maximum (FWHM) of the Doppler-broadened profile Δv_D is directly related to the translational temperature:

$$\Delta v_D = v_0 \sqrt{\frac{8k_B T_t \ln(2)}{mc^2}} = 7.1623 \times 10^{-7} v_0 \sqrt{\frac{T_t}{M}}$$
 (4)

where v_0 is the line-center frequency, M is the atomic mass, $k_{_{\mathcal{B}}}$ is the Boltzmann constant, and c is the speed of light. By fitting a Gaussian profile to the measured absorbance spectrum, the translational temperature can be directly calculated from the FWHM.

The number density is determined from the integrated absorbance. Integrating the absorbance over the entire absorption profile eliminates the influence of the lineshape function due to its normalization ($\int \phi_{\nu} d\nu = 1$). This yields the number density of the lower state:

$$n_{l} = \frac{A_{int}}{S_{lu} \cdot L} = \frac{\int k_{v} \, dv}{\lambda_{0}^{2} \cdot (g_{u} \mid g_{l}) \cdot (A_{ul} \mid 8\pi c)}$$
 (5)

The line strength S_{lu} is a function of fundamental spectroscopic constants and temperature, When T_{exc} is much smaller than $hc / \lambda_0 k_B$, S_{lu} can be expressed by the following equation:

$$S_{lu} = \frac{\lambda_0^2}{8\pi c} \cdot A_{ul} \cdot \frac{g_u}{g_l} \tag{6}$$

where λ_0 is the transition wavelength, g_i and g_u are the degeneracies of the lower and upper states, and A is the Einstein coefficient for spontaneous emission.

To obtain the total number density of the species, we assume the gas is in local thermodynamic equilibrium (LTE). Under this assumption, the population of energy levels follows the Boltzmann distribution. The relationship between the lower-state density n_{l} and the total density n_{0} is:

$$\frac{n_{l}}{n_{0}} = \frac{g_{l}}{Q(T)} \exp\left(-\frac{E_{l}}{k_{B}T}\right) \tag{7}$$

Where E_{j} is the energy of the lower state and Q(T) is the temperature-dependent partition function, which accounts for the population distribution across all electronic states.

For this investigation, specific transitions for atomic oxygen and nitrogen were selected for their strong absorption and SMALL spectral interference. We targeted the O transition at 777.19 nm (${}^5S_2 \rightarrow {}^5P_3$) and the N transition at 868.03 nm (${}^4P_{5/2} \rightarrow {}^4D_{7/2}$). The fundamental spectroscopic parameters for these transitions are summarized in Table 1.

Table 1. basic spectral parameters of selected electronic transition of oxygen and nitrogen atoms

Atom	λ_0 / nm	A_{ul} / s ⁻¹	$g_{_{I}}$	$g_{_{u}}$	<i>E</i> ,/ eV	E_u / eV
0	777.19	3.69e7	5	7	9.15	10.74
N	868.03	2.53e7	6	8	10.34	11.76

3. Experimental Setup

3.1. C/SiC Material

The material investigated in this study was a carbon fiber-reinforced silicon carbide (C/SiC) ceramic matrix composite, fabricated using the Chemical Vapor Infiltration (CVI) process.

The C/SiC composite was machined into disk-shaped specimens for testing. The specimen measured 8 mm in thickness, with a front surface diameter of 40 mm and a rear surface diameter of 42 mm. The mass of the specimens was 21.87 g. For the experiment, the specimen was secured in a custom-designed, water-cooled holder and positioned 100 mm from the exit nozzle of the plasma facility. A photograph of the specimen and a schematic of the mounting configuration are shown in Fig. 1(a) and (b), respectively.

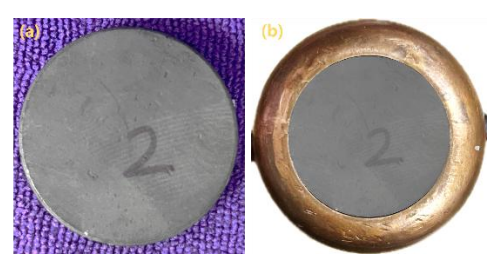


Fig. 1 CVI-C/SiC material sample and installation schematic

3.2. Experimental Facility and Procedure

The experiments were conducted in the 1.2 MW Inductively Coupled Plasma (ICP) wind tunnel at the China Academy of Aerospace Aerodynamics (CAAA). This ground-test facility simulates the reentry environment of hypersonic vehicles by generating a stable, high-enthalpy plasma jet that is free from electrode contamination. Its capabilities are particularly well-suited for evaluating the performance of thermal protection materials and investigating gas-surface interaction mechanisms. A detailed description of the facility's architecture and plasma generation process is available in previous works [22-23]. The generated plasma jet is accelerated through a water-cooled nozzle before entering the test chamber. The chamber, with dimensions of 1.2 m \times 1.2 m \times 2 m, is equipped with multiple quartz windows to accommodate various optical diagnostic instruments

The specific operating conditions for this study are detailed in Table 2. The total pressure within the ICP generator was monitored using a pressure transducer.

Test material	Stagnation enthalpy H_0 / MJ·kg ⁻	Total pressure P_0 / kPa	Heat flux q_{cw} / MW·m ⁻²	Heating time / s	Temperatu re before jump / K	Temperatu re after jump / K
C/SiC	42.8	4.8	3.6	160	2000	2400

Table 2. Experimental conditions

During the experiments, the surface temperature at the specimen's stagnation point was monitored in real-time using a single-color optical pyrometer (FLUKE Endurance Series, E1MH-F2-L-0-0, 500-3000°C). The pyrometer was aimed at the specimen through a quartz window, with the material's surface emissivity set to 0.85 and a data acquisition rate of 100 Hz. The experimental setup, including the specimen's mounting configuration within the test chamber, is depicted in Fig. 2.

To effectively observe the temperature jump on the C/SiC surface, a two-stage thermal loading procedure was designed. First, the C/SiC specimen was subjected to an initial thermal load. This stage was intended to activate the material's surface, creating the physicochemical conditions for the subsequent temperature jump. After the specimen cooled to room temperature, it was exposed to a second thermal load under identical plasma conditions. During this second stage, the characteristic temperature jump was successfully observed. Consequently, the data analysis and mechanistic discussion in this paper focus primarily on this second thermal loading stage to investigate the mechanism and evolution of temperature jump.

Following the experiments, the surface morphology of the specimen was characterized using a Scanning Electron Microscope (SEM) to correlate the observed temperature jump behavior with changes in the material's ablation morphology.

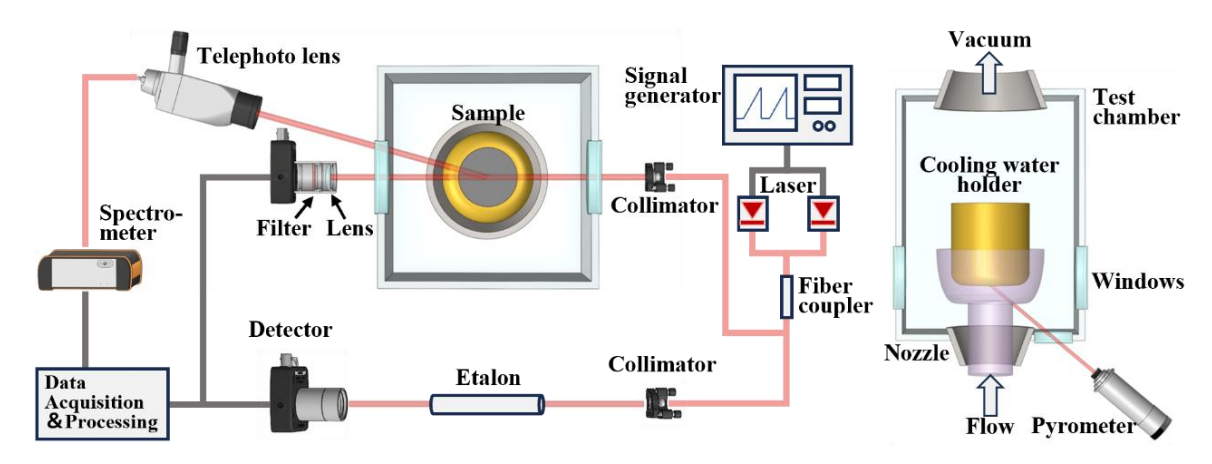


Fig. 2 Schematic layout of the experimental system

3.3. Spectroscopic Diagnostic Systems

The arrangement of the spectroscopic measurement systems is illustrated in Fig. 2. Two complementary optical techniques, Laser Absorption Spectroscopy (LAS) and Optical Emission Spectroscopy (OES), were employed for in-situ characterization of the chemically reacting boundary layer adjacent to the specimen surface

The LAS system was implemented to quantify the translational temperature and number densities of atomic oxygen (O) and nitrogen (N) adjacent to the specimen surface. The measurement setup involved two tunable diode lasers: a 777.19 nm Distributed Bragg Reflector (DBR) laser for O and an 868.03 nm Distributed Feedback (DFB) laser for N. A function generator (Tektronix, AFG3101) produced a 100 Hz sawtooth signal that modulated two laser controllers (Thorlabs, ITC4001), which in turn scanned the output wavelength of each laser across the respective atomic absorption lines. The modulated beams were merged into a single optical fiber, enabling simultaneous O/N measurements. The combined beam was then split; one part was collimated and directed perpendicularly through the plasma flow, passing the specimen's central axis and was near its surface. The other part was directed through an etalon for precise frequency calibration. The transmitted laser signal was captured by a photodetector (Thorlabs, PDA36A2). To improve the signal-to-noise ratio and minimize interference from plasma emission, a plano-convex lens and a narrow bandpass filter were installed in front of the detector.

Complementing the absorption measurements, OES was used to monitor the radiative intensity of species within the boundary layer, providing insight into the composition and chemical state of the plasma. Plasma radiation from the region near the specimen's stagnation point was collected by a long-focal-length lens (Gigahertz-Optik, LDM-9811; f=1.3 m). The collected light was then transmitted via a 1-to-4 optical fiber to a bank of four spectrometers (AvaSpec-UL2048CL-RS EVO). This setup enabled the acquisition of emission spectra covering a broad wavelength range from 300 to 890 nm.

4. Results and Discussion

4.1. Results of Initial Thermal Load

This section describes the material's thermochemical response during the initial stage of thermal loading. Since this phase did not exhibit a temperature jump, the discussion remains relatively concise and serves as a foundational reference for the subsequent analysis of temperature jump.

The evolution of the specimen's surface temperature during this initial exposure is presented in Fig. 3. Following a rapid transient heating period, the temperature reached and maintained a stable plateau at approximately 1950 K.

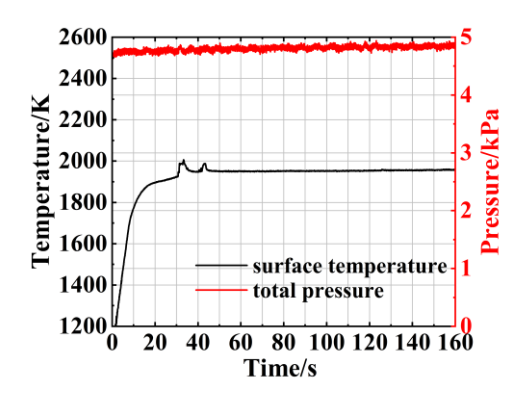


Fig. 3 Surface temperature and pressure in the initial thermal load

Concurrently, Fig. 4 shows the spectroscopic measurements from the near-body boundary layer. The normalized radiative intensities of key species, namely Si, CN, N_2^+ , N, and O, were observed to rise sharply at first, reach a peak, and then gradually decline over the course of the test. During the same period, the translational temperature and the number densities of atomic O and N inferred from LAS remained remarkably stable, indicating a steady gas-phase environment near the surface.

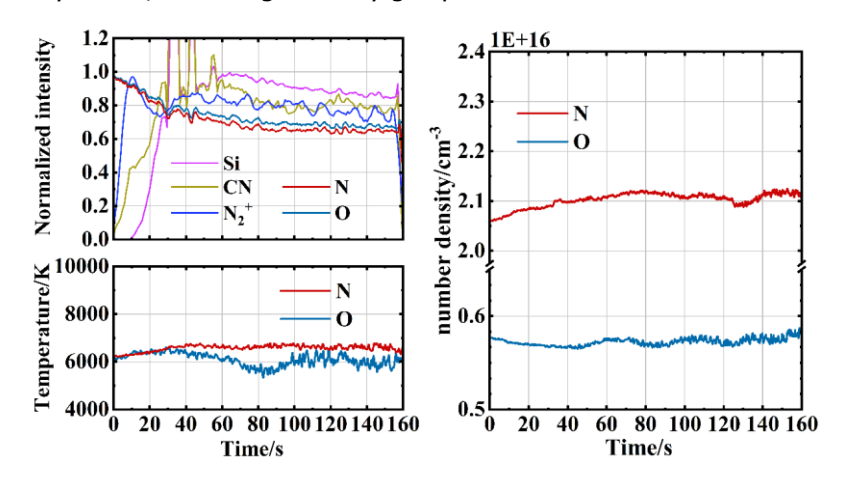


Fig. 4 Normalized radiative intensity, translational temperature, and number density in the initial thermal load

4.2. Results of Temperature Jump

4.2.1 Surface Temperature Jump and Ablation Morphology

The temperature jump on the C/SiC specimen surface was distinctly captured during the second thermal loading experiment, as shown by the pyrometer data in Fig. 5(a). The figure also includes the total pressure within the test chamber, which stabilized shortly after the test began; this moment is defined as t = 0. The total test duration was approximately 160 s.

The specimen's surface temperature profile can be divided into three phases. In the first 20 seconds, the surface heated rapidly. It then entered a stable plateau phase, maintaining a temperature of approximately 2000 K. At t ≈ 105 s, a significant temperature jump occurred: the surface temperature abruptly increased from 2000 K to 2400 K within about 10 seconds. This elevated temperature was sustained until the conclusion of the experiment. This behavior is consistent with temperature jump phenomena reported in previous studies [7-12].

This dramatic thermal event resulted in a significant change in the material's surface ablation behavior, as illustrated by the macroscopic photographs in Fig. 5(b), 5(c), and 5(d). For comparison, the prejump morphology (Fig. 5(c)) was obtained from a separate, identical C/SiC specimen tested under the same conditions, but with the exposure intentionally terminated just before the jump. The pristine specimen (Fig. 5(b)) had a smooth, dense surface. After exposure but before the jump, a white oxide layer formed on the surface with only minor mass change. In stark contrast, after the temperature jump (Fig. 5(d)), the specimen's central region showed severe ablation, characterized by exposed fibers.

HiSST-2025-#296 Page | 7

Some residual white material remained near the periphery. The specimen's mass decreased from 21.87 g to 21.01 g, corresponding to a mass loss of approximately 4%. It should be noted that the less pronounced reaction features at the edges are attributed to the water-cooled holder, which provided more efficient heat dissipation in that region.

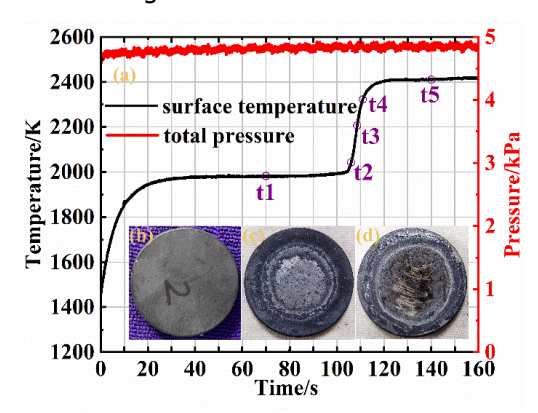


Fig. 5 Surface temperature and macroscopic photographs of the sample: a) surface temperature, b) before experiment, c) before temperature jump, d) after temperature jump

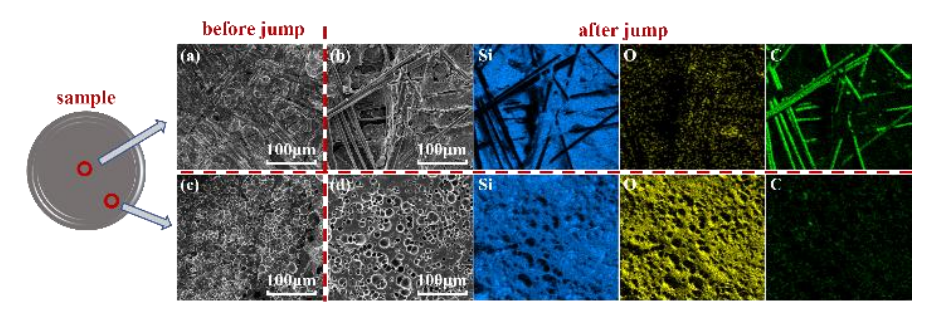


Fig. 6 SEM and EDS results of the C/SiC sample after experiment: a) central region before temperature jump, b) central region after temperature jump, c) edge region before temperature jump, d) edge region after temperature jump

To investigate the microstructural and chemical changes associated with the temperature jump, the specimen surfaces were analyzed using Scanning Electron Microscopy (SEM). Fig. 6 presents a comparative analysis of the sample's central and edge regions, corresponding to the macroscopic states shown in Fig. 6(c) (pre-jump) and 6(d) (post-jump).

Prior to the temperature jump (Fig. 6(a) and 6(c)), the specimen surface was characterized by the formation of a protective silica (SiO₂) layer, a product of passive oxidation that covered nearly the entire heated area:

$$SiC(s) + 3O(g) = SiO_2(s) + CO(g)$$

In the central, high-temperature region (Fig. 6(a)), this SiO_2 layer appeared as a continuous, fused film covering the underlying material. In contrast, the cooler edge region (Fig. 6(c)) exhibited a different morphology, with the SiO_2 forming distinct, bubble-like clusters.

Following the temperature jump, the surface morphology underwent a dramatic transformation (Fig. 6(b) and 6(d)). In the central region, the protective SiO_2 layer had almost completely disappeared. The underlying SiC matrix was severely ablated, exposing the carbon fiber substrate. This indicates a transition to an active oxidation regime, which consumes the SiC and produces volatile silicon monoxide (SiO) gas:

$$SiC(s) + 2O(g) = SiO(g) + CO(g)$$

At the specimen's edge, while some SiO_2 remained, its structure had evolved. The post-jump morphology showed a significant increase in porosity compared to the pre-jump state (Fig. 6(d)). This porous structure is attributed to the intensified gas-producing reactions at the elevated post-jump temperatures. The morphological differences between the center and the edge are consistent with the surface temperature gradient induced by the water-cooled holder.

In summary, the SEM analysis provides direct microstructural evidence that the temperature jump phenomenon marks a critical transition in the gas-surface interaction mechanism. The material shifts from a passive oxidation regime, characterized by a protective liquid SiO₂ layer, to an active oxidation regime, dominated by the rapid consumption of SiC and the release of gaseous products. This transition is fundamentally linked to the sharp increase in surface temperature.

The changes in material surface properties reflecting a shift in oxidation mechanisms are considered one of the key factors triggering temperature excursions. As noted above, the coupled gas—solid effects on the material surface — including oxidation, catalysis, and thermal decomposition — jointly contribute to the high complexity of the temperature-rise process. To thoroughly elucidate this dynamic evolution, quantitative parameter-analysis methods with time-resolved capability are urgently needed.

The observed transition in the oxidation mechanism, inferred from the changes in surface properties, is considered a primary driver of the temperature jump. However, as previously discussed, the temperature jump is a highly complex process resulting from the interplay of multiple coupled gassurface effects, including oxidation, catalysis, and pyrolysis. To deconstruct this dynamic evolution and gain a deeper mechanistic understanding, a quantitative analysis with temporal resolution is essential.

4.2.2 Near-body Translational Temperature and Number Density of O and N Atoms

The LAS diagnostics captured the dramatic evolution of the gas-phase boundary layer during the temperature jump. As shown in Fig. 7, the absorption lines of O and N atoms broadened significantly during the event, directly indicating a sharp rise in their translational temperature. The high accuracy of the Gaussian fits (residuals $< \pm 0.005$) validates the quantitative analysis.

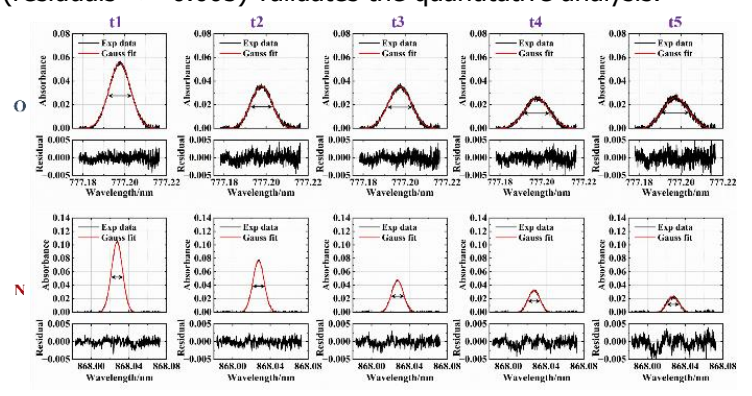


Fig. 7 Experimental atomic absorption lines of O/N, Gaussian fitted signals, and fitting residuals

The inverted, time-resolved data are presented in Fig. 8. The results show a clear, synchronous response with the surface temperature. Before the jump (t < 105 s), the translational temperature and number density were relatively stable. At the onset of the jump (t \approx 105 s), both the translational temperature and the number densities of O and N atoms increased sharply. After a $\sim\!10$ -second transition, they settled into a new, stable, high-energy state. A subtle but important feature of this transition is that the O atom number density increased more gradually than the N atom density.

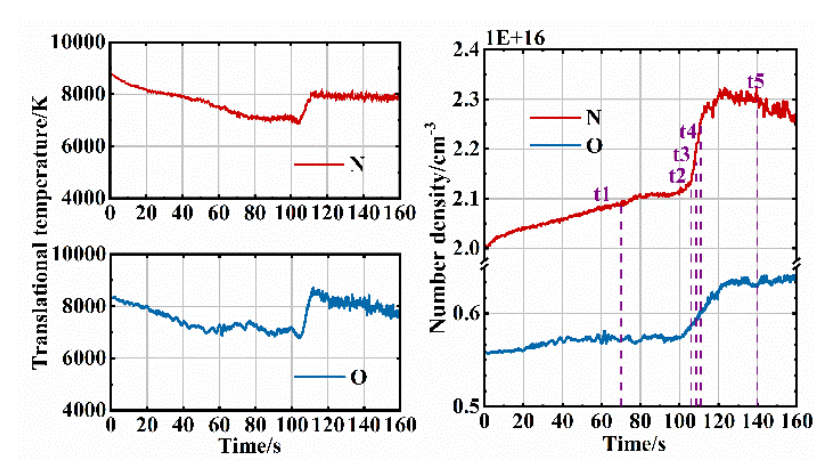


Fig. 8 Translational temperature and number density of O/N atoms

The observed trends in atomic species can be explained by the evolving surface chemistry. At the beginning of the experiment, the specimen surface was not yet fully covered by a protective SiO_2 layer. This exposed SiC surface facilitates the consumption of O and N atoms through two primary pathways. First, the SiC acts as a catalyst for atomic recombination reactions $(O+O\rightarrow O_2 \text{ and } N+N\rightarrow N_2)$. Second, the passive oxidation of SiC consumes atomic oxygen to form a stable, condensed SiO_2 layer, effectively sequestering oxygen atoms from the gas phase. This interpretation is consistent with the SEM observations of the white oxide film (Fig. 6(a), 6(c)), confirming that the initial phase is dominated by passive oxidation.

The time-resolved LAS data provide a dynamic perspective that complements the static SEM morphologies. As the SiO₂ layer progressively forms and covers the surface, it effects the reaction dynamics. Compared to SiC, SiO₂ has a significantly lower catalytic efficiency for atomic recombination, thereby suppressing this consumption pathway. Furthermore, the growing oxide layer acts as a diffusion barrier, physically hindering the underlying SiC from reacting with the plasma. With both reaction pathways inhibited, the consumption rate of O and N atoms at the surface decreases. This shift in reaction kinetics is directly reflected in our LAS measurements as a gradual increase in the near-body atom number densities and a corresponding decrease in their translational temperature, as less chemical energy is released at the surface.

The temperature jump is initiated when the protective SiO_2 layer fails under sustained thermal and chemical attack, leading to a transition from passive to active oxidation, consistent with our SEM findings. This breakdown is driven by processes such as the reaction between silicon carbide and silica $(SiC(s)+SiO_2(s)=2SiO(g)+C(s))$ and by erosion from atomic oxygen $(SiO_2(s)+O(g)=SiO(s)+O_2(g))$ [24-25].

This regime shift fundamentally alters the gas-surface interaction. The production and subsequent dissociation of volatile SiO (g) leads to a less efficient net consumption of O atoms at the surface compared to the passive regime. This reduced consumption is observed as a sharp increase in the O atom number density. Concurrently, the transition to the active oxidation regime signifies a dramatic acceleration of the overall surface reaction rate, causes a dramatic spike in the local gas-phase translational temperature, which in turn drives the macroscopic surface temperature jump.

The distinct response of nitrogen atoms corroborates this interpretation. The N atom density, governed mainly by catalysis and nitridation, shows a steeper increase. This suggests that its interaction pathway is more straightforward, in contrast to the complex, multi-step reaction network involving oxygen, which results in a more gradual density increase during the transition.

4.2.3 Near-body Radiative Intensity Variation of Chemical Reaction Species

To complement the analysis of reactant consumption, Optical Emission Spectroscopy (OES) was used to characterize the evolution of key reaction products, particularly atomic silicon (Si) and the cyanogen radical (CN). Fig. 9 displays representative emission spectra in the 375–395 nm wavelength range at five characteristic moments during the test (as marked in Fig. 5(a)). Distinct characteristic lines for both Si and CN are clearly visible, and their intensities evolve significantly over time. A dramatic intensification of both signals is evident immediately following the temperature jump. Notably, during the pre-jump phase, characteristic emission from silicon monoxide (SiO) was also detected.

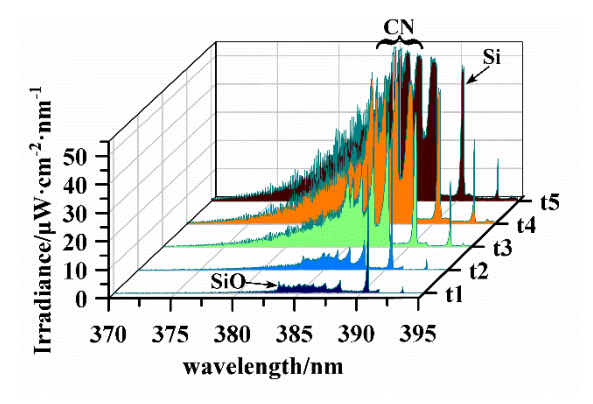


Fig. 9 Radiation spectral lines of 375nm ~ 395nm at five characteristic moments

Fig. 10 Si and CN variation of normalized radiation intensity

The temporal evolution of these products is quantified by their normalized, integrated emission intensities, as plotted in Fig. 10. The Si signal is notably absent during the first ~ 10 seconds of exposure, a period that corresponds to the initial passive oxidation regime where silicon is sequestered into the condensed SiO₂ layer. This behavior aligns with the pre-jump SEM analysis and the initial consumption of O and N atoms. As the surface temperature rises, the emergence of the Si signal suggests the onset of localized active oxidation and reactions involving the newly formed SiO₂ layer. This interpretation is supported by the direct detection of gaseous SiO in the emission spectra and explains the appearance of atomic Si in the boundary layer. The subsequent stabilization of the Si signal can be linked to the formation of a molten SiO₂ film that covers surface pores and moderates the reaction rate, corroborating the fused morphology observed via SEM. In contrast, the CN signal, originating from reactions between carbon and atomic nitrogen, is present from the early stages of the experiment.

At the moment of the temperature jump (t ≈ 105 s), a critical and synchronous intensification of both the CN and Si emission signals occurs. Following this sharp peak, both signals exhibit a continuous decay until the end of the test, a transient behavior consistent with prior observations of this phenomenon. The spike and subsequent decay of the Si signal are indicative of the rapid production of gaseous SiO during the active oxidation phase, followed by the gradual depletion of the SiC reactant near the surface. Simultaneously, the intense flare of CN emission corresponds precisely to the period when the protective SiC/SiO₂ layers are stripped away, exposing the underlying carbon fibers to the nitrogen-rich plasma and leading to enhanced nitridation and oxidation reactions.

5. Conclusion

This study investigated the mechanism of the temperature jump on C/SiC composites under high-enthalpy aerothermal conditions, a critical issue for the thermal protection systems of reusable spacecraft. An experimental scenario was successfully designed in a 1.2 MW plasma wind tunnel (enthalpy: 42.8 MJ/kg; heat flux: 3.6 MW/m²) to replicate the event, inducing a surface temperature jump from approximately 2000 K to 2400 K over 160 s. By employing including Laser Absorption Spectroscopy (LAS), Optical Emission Spectroscopy (OES), and Scanning Electron Microscopy (SEM), we have investigated the coupled gas-surface interactions that govern this complex process. The primary conclusions are as follows:

- A transition from passive to active oxidation was observed during the temperature-jump. SEM images taken before the temperature jump show a layer of SiO₂ on the surface. After the temperature jump, the central region no longer exhibited SiO₂, and the SiC layer displayed significant ablation with the carbon-fiber substrate exposed. Comparison of pre- and post-jump micrographs indicates that failure of the protective SiO₂ scale triggered the oxidation mode transition.
- The response characteristics of near-body atomic oxygen and nitrogen densities and translational temperature during the temperature jump were revealed. Quantitative TDLAS measurements show that, during the temperature jump, both the translational temperature and the number densities of near-body O and N atoms undergo simultaneous, abrupt increases. This behavior is attributed to a reduced overall consumption rate of gas-phase reactants (O and N atoms) under the active-oxidation regime. Notably, the increase in N atom density is steeper than that of O atoms, which is consistent with the relatively simpler reaction pathways involving nitrogen atoms.

HiSST-2025-#296
New Insights into The Temperature Jump of C/SiC Composites under Extreme Aerothermal Conditions

• The change in reaction mode during the temperature jump was corroborated by the occurrence of intense gas—surface reactions. Optical emission spectroscopy (OES) detected synchronous surges in the radiative intensities of Si atoms and CN species coincident with the temperature jump. This observation is consistent with active oxidation producing substantial gas-phase products (e.g., SiO) and with exposure of the carbon substrate that subsequently reacts with incoming nitrogen atoms.

In summary, by integrating time-resolved, quantitative measurements of reactant densities with spectral monitoring of reaction products and detailed microstructural analysis, this research offers a new and detailed perspective on the gas-surface coupling that governs this phenomenon, providing valuable data to advance the understanding and predictive modeling of C/SiC materials in extreme aerothermal environments.

Acknowledgements

This work is supported by the National Natural Science Foundation of China (Grant Nos. 92271117, 12402395), and the Strategic Priority Research Program of the Chinese Academy of Sciences (rant No. XDB0620202).

References

- 1. Buffenoir, F., Zeppa, C., Pichon, T., et al.: Development and flight qualification of the C-SiC thermal protection systems for the IXV. Acta Astronaut. 124, 85–89 (2016)
- 2. Balat-Pichelin, M., Charpentie, L., Panerai, F., et al.: Passive/active oxidation transition for CMC structural materials designed for the IXV vehicle re-entry phase. J. Eur. Ceram. Soc. 35, 487–502 (2015)
- 3. Yang, L.W., Jing, L., Zhang, J., et al.: Excellent ablation resistance and reusability of silicon carbide fiber reinforced silicon carbide composite in dissociated air plasmas. J. Eur. Ceram. Soc. 43, 2275–2281 (2023)
- 4. Sakraker, I., Asma, C.O.: Experimental investigation of passive/active oxidation behavior of SiC based ceramic thermal protection materials exposed to high enthalpy plasma. J. Eur. Ceram. Soc. 33(2), 351–359 (2013)
- 5. Panerai, F., Helber, B., Chazot, O., et al.: Surface temperature jump beyond active oxidation of carbon/silicon carbide composites in extreme aerothermal conditions. Carbon 71, 102–119 (2014)
- 6. Lacombe, A., Lacoste, M.: Investigation of C/SiC "breakingpoint" under arc jet environment at NASA JSC. J. High Temp. Chem. Process. 3(3), 285–296 (1994)
- 7. Herdrich, G., Fertig, M., Löhle, S., et al.: Oxidation behavior of siliconcarbide-based materials by using new probe techniques. J. Spacecr. Rockets 42(5), 817–824 (2012)
- 8. Herdrich, G., Auweter-Kurtz, M., Fertig, M., et al.: Catalytic and oxidative behaviour of silicon carbide based materials for thermal protection materials. In: 55th International Astronautical Congress, Vancouver, Canada (2004)
- 9. Laux, T., Herdrich, G., Auweter-Kurtz, M.: Oxidation behavior of sintered silicon carbide in various plasma wind tunnels. In: 4th European Workshop on Hot Structures and Thermal Protection Systems for Space Vehicle, Palermo, Italy (2002)
- 10. Hald, H., Ullmann, T.: Reentry flight and ground testing experience with hot Structures of C/C-SiC Material. In: 44th AIAA/ASME/ASCE/AHS Structures, Structural Dynamics, and Materials Conference, Norfolk, Virginia (2003)
- 11. Hald, H.: Operational limits for reusable space transportation systems due to physical boundaries of C/SiC materials. Aerosp. Sci. Technol. 7, 551–559 (2003)
- 12. Panerai, F., Chazot, O., Helber, B.: Gas/surface interaction study on ceramic matrix composite thermal protection system in the vki plasmatron facility. In: 42nd AIAA

- Thermophysics Conference, Honolulu, Hawaii (2011)
- 13. Panerai, F., Chazot, O.: Plasma Wind Tunnel Testing as Support to the Design of Gas-Surface Interaction In-Flight Experiments. In: 17th AIAA International Space Planes and Hypersonic Systems and Technologies Conference, San Francisco, California (2011)
- 14. Marschall, J., Pejaković, D.A., Fahrenholtz, W.G., et al.: Temperature jump phenomenon during plasmatron testing of zrb2-sic ultrahigh-temperature ceramics. J. Thermophys. Heat Transf. 26(4), 559–572 (2012)
- 15. Yang, Y.J., Zhang, S.H., Yang, L.W., et al.: 'Temperature jump' mechanism of silicon carbide based thermal protection material in arc-jet flow. Int. J. Therm. Sci. 202, 109064 (2024)
- 16. Zhang, X.H., Du, B.H., Hu, P., et al.: Thermal response, oxidation and ablation of ultra–high temperature ceramics, C/SiC, C/C, graphite and graphite–ceramics. J. Mater. Sci. Technol. 102, 137–158 (2022)
- 17. Luo, L., Wang, Y.G., Liu, L.P., et al.: Ablation behavior of C/SiC composites in plasma wind tunnel. Carbon 103, 73–83 (2016)
- 18. Burghaus, H., Kaiser, C.F., Pagan, A.S., et al.: Aerothermodynamic characterization of inductively generated carbon dioxide plasma by laser absorption spectroscopy. J. Thermophys. Heat Transf. 38(1), 98–108 (2024)
- 19. Finch, P.M., Girard, J.J., Schwartz, T., et al.: Measurements of T5 Shock Tunnel Freestream Temperature, Velocity, and Composition. AIAA J. 61(4), 1555–1578 (2023)
- 20. Matsui, M., Komurasaki, K., Arakawa, Y.: Laser absorption spectroscopy in high enthalpy flows. In: 38th AIAA Thermophysics Conference, Toronto, Canada (2005)
- 21. Merrell, D.P., Drescher, D., Granowitz, Z.N., et al.: Simultaneous, pathlength-amplified laser absorption measurements of excited air species in a shock tube. In: AIAA SCITECH 2025 Forum, Orlando, FL (2025)
- 22. Fang, S.H., Lin, X., Zeng, H., et al.: Gas—surface interactions in a large-scale inductively coupled plasma wind tunnel investigated by emission/absorption spectroscopy. Phys. Fluids 34, 082113 (2022)
- 23. Fang, S.H., Lin, X., Yang, J.N., et al.: Spectral insight into the interface evolution of a carbon/carbon composite under high-enthalpy, nonequilibrium flow. Phys. Fluids 35, 102116 (2023)
- 24. Harder, B., Jacobson, N., Myers, D.: Oxidation Transitions for SiC Part II. Passive-to-Active Transitions. J. Am. Ceram. Soc. 96(2), 606–612 (2013)
- 25. Glass, D.E.: Physical Challenges and Limitations Confronting the Use of UHTCs on Hypersonic Vehicles. In: 17th AIAA International Space Planes and Hypersonic Systems and Technologies Conference, San Francisco, California (2011)